

AN UNCONVENTIONAL TRANSITION RADIATION DETECTOR

ABSTRACT

A transition radiation detector operating at low gas pressures was built at Yerevan and tested at FERMILAB. At low pressure, total $\frac{dE}{dx}$ is decreased without loss of efficiency for transition radiation x-rays. Data with π 's and p's at 40, 100 and 200 GeV/c momenta are presented. The data shows that 0.5% overlap between π 's and p's may be achieved at 40 GeV/c with a 2 m long detector.

A. G. Oganessian, A. T. Sarkissian
Yerevan Physics Institute

M. Atac
Fermi National Accelerator Laboratory

April 5, 1977

AN UNCONVENTIONAL TRANSITION RADIATION DETECTOR

The identification of hadrons in the energy range between 30 GeV and 400 GeV by means of conventional methods (Cerenkov counters, counters based on the relativistic rise of ionization losses and known versions of X-Ray Transition Radiation (XTR)-detectors) is known to be a rather difficult and even impractical task.^{1,4}

At Yerevan Physics Institute a novel XTR-detector was proposed⁵ which is based on the method of the energy deposition and it is capable of the identification of hadrons in the momentum range $30 \leq p \leq 400$ GeV/c. In the proposed detector, the XTR radiator and proportional chambers were combined to reduce the probability of the absorption of transition radiation within the radiator and to increase the number of quanta absorbed in the gas mixture. This fact, together with the choice of the reduced pressure of the filling gas of the chamber allowed to increase the share of the transition radiation in the total energy deposition in the gas mixture.

Such XTR-detector was made at Yerevan Physics Institute and investigated at the Fermi National Accelerator Laboratory. The experimental layout and chamber are shown in Fig. 1. The chamber consists of 18 sensitive planes separated by double-side coated aluminized mylar. The mylar has a thickness of $5\mu\text{m}$ and the thickness of aluminum on each side of the mylar is 250 \AA . The diameter of sense wires is $25\mu\text{m}$ and spacing is 2 mm. All planes were mounted in a stainless steel gas enclosure with mylar windows. The typical pressure of the gas mixture (80% Xe + 20% CO₂) was

20 ÷ 30 mm Hg.

All signal wires were connected together to the input of a low noise charge sensitive preamplifier. The signal was carried from preamplifier to the amplifier and further to the multichannel pulse height analyzer. The gate of the latter at 40 GeV/c run was triggered by coincidence (or anti-coincidence) between the scintillator telescope ($S1 \cdot S2 \cdot S3 \cdot S4 \cdot \bar{V}$) and the threshold Cerenkov counter. During the 100 GeV/c and 200 GeV/c runs, analyzer was triggered by coincidence between the telescope and differential Cerenkov counter (for the proton runs) or DISC (for the pion run). The proton and pion runs took turns every other hour to eliminate the apparatus distortions. An Fe^{55} X-Ray source was used between accelerator cycles to measure variations of the gas gain. A typical Fe^{55} spectrum is shown in Fig. 2.

Figures 3, 4, and 5 show the pulse height distributions for pions and protons at 40, 100, and 200 GeV/c respectively, at the pressure of the gas mixture 20 mm Hg. All data were corrected for systematic drifts using Fe^{55} measurements. They show that all the distributions have almost gaussian shape without long "Landau tail" except for the 200 GeV/c proton run. The explanation of this phenomena probably is that the ionization δ -electrons liberated by the incident particle which are the cause of the long "Landau tail" are captured by dense mylar foils without significant ionization of the gas. The wider distributions at 100 GeV/c and 200 GeV/c are the result of a) the increasing of the XTR share in the total energy yield in the gas and b) two mylar planes failed. Figures 3 thru 5 make it clear that at the pressure 20 mm π/P separation is on the order of a full width at half maximum.

Figure 6a represents the most probable value of the energy deposition in a single cell of XTR-detector behaves as a function of Lorentz-factor $\gamma = E/mc^2$, at the different conditions. The lower curve corresponds the ionization losses in arbitrary units at NTP according to Allison, et al. [2]. The middle curve represents the predictions of Steinheimer [6] at the pressure 20 mm Hg. The dashed curve takes into account XTR deposit. In contrast to case of atmospheric pressure, the reduced pressure shifted Fermi plateau to higher energies as it follows from Fig. 6a. Additional rise in the energy dependence comes from XTR in the Lorentz-factor region $\gamma > 2 \cdot 10^2$. Our experimental data (open circles) are in agreement with the theoretical predicitions.

As was to be expected, both the low pressure and XTR allowed to improve the ratio of ionization (peak position) between protons and pions. Indeed, as shown in Fig. 6b, the ratio of ionization W_π/W_p in the Xenon at NTP (solid curve) is smaller than at the low pressure (dashed curve). Meanwhile, in this detector W_π/W_p is not only higher, but at $p > 100$ GeV/c, it begins to increase (open circles).

Using the experimental results presented in Figures 3 thru 5, a Monte Carlo program was simulated for 10 above described XTR-detector samples. To improve the mass resolution, we discarded the largest 4 pulse heights and therefore we took the mean of this set of 6 pulse heights for each particle. An equal number of protons and pions was assumed. Figures 7a, 8 and 9 show the separation of pions and protons achieved this way. The overlapping areas of the proton and pion distributions are about 4-7% at all measured energies.

Figure 7b shows the mean of the 6 smallest signals expected from such a device in the case of the mixture of pions and protons in the ratio 10:1 at 40 GeV/c. The optimum cut between pions and protons would result in a loss of about 12% protons into the pion peak and 12% pions mis-identified as protons. Finally, we note, that the overlapping area is roughly 0.5% in the case of 20 XTR-detector samples for a total length of about 2m.

Our results suggest that at the momenta $p < 100$ GeV/c, the new XTR-detector is as applicable as Cerenkov counters and exploitation of ionization losses in MWPC. At the higher energies when these techniques are often inapplicable, XTR-detector becomes more profitable.

Acknowledgments

The authors would like to express their thanks to Drs. E. Goldwasser, A. L. Read and R. Shafer for their support and Dr. M. Johnson and Dr. H. Haggerty and M. Haldeman for their help at the Fermi National Accelerator Laboratory. We would also like to thank Prof. A. Tz. Amatuni for his support of this project and K. G. Antonian, A. T. Avundzian, A. T. Kazarian, S. A. Kankanian and A. G. Tamanian for their part in building the chamber.

References

1. M. Benot, L. Litt, R. Meunier, CERN/ECFA/F2/4, VI.
2. W. W. M. Allison, C. B. Brooks, J. N. Bunch, R. W. Fleming, R. K. Yamamoto, Nucl. Instr. and Meth., 133 (1976) 325.
3. L. C. L. Yuan, P. W. Alley, G. F. Dell, H. Uto, BNL (1965)1.
4. R. Bosshard, J. Fischer, S. Iwata, V. Radeka, C. L. Wang, M. Atac, Nucl. Instr. and Meth., 127 (1975) 141.
5. K. G. Antonyan, A. T. Avundzyan, S. P. Kazaryan, S. A. Kankanyan, A. G. Oganessian, A. G. Tamanyan, Preprint EFI-130 (1975), Yerevan.
6. R. M. Sternheimer and R. F. Peierls, Phys. Rev., B3 (1971) 3681.

Figure Captions

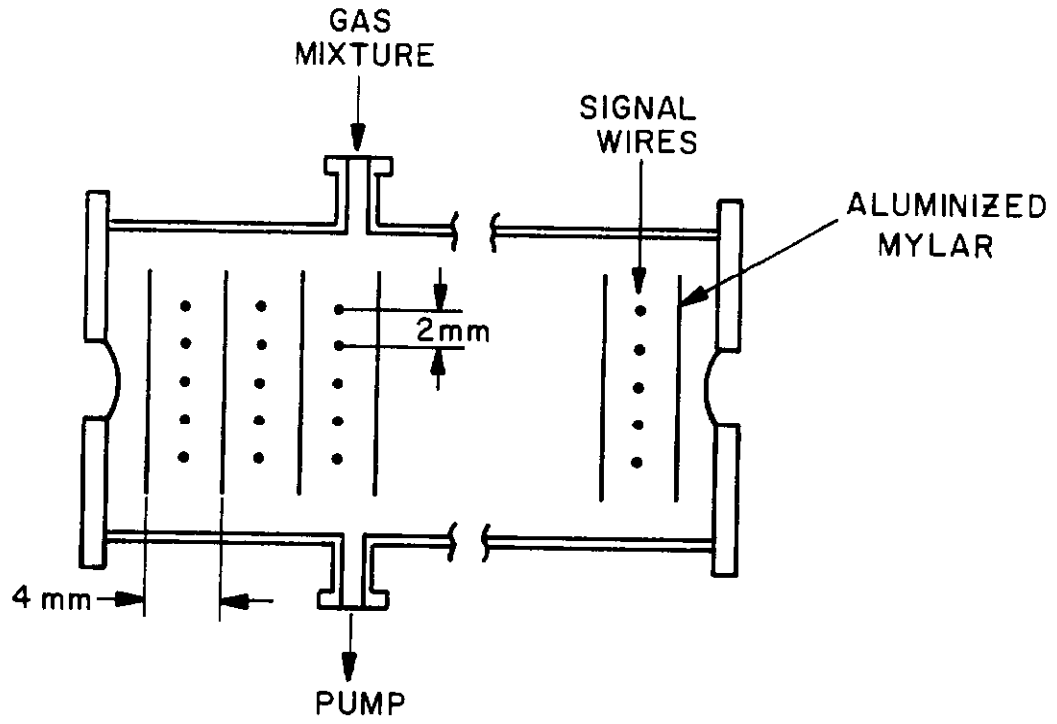
- Fig. 1(a) Schematic side view of XTR-detector.
 1(b) Beam diagram.
- Fig. 2 Fe⁵⁵ spectrum taken between accelerator cycles.
- Fig. 3 The pulse height distributions for π and p at 40 GeV/c.
- Fig. 4 The pulse height distributions for π and p at 100 GeV/c.
- Fig. 5 The pulse height distributions for π and p at 200 GeV/c.
- Fig. 6(a) A comparison of the relativistic rise of the most probable energy depositions at various pressures under XTR influence.
- 6(b) π/p ratio of ionization as a function of the momenta at the different pressures and in the XTR-detector.
- Fig. 7(a) The pulse height distributions of the mean of the smallest 6 out of 10 pulses in flux ratio $\pi/p = 1:1$ at 40 GeV/c
- 7(b) The same distributions in flux ratio $\pi/p = 10:1$.

Figure Captions

Fig. 8 The pulse height distributions of the mean of the
 smallest 6 out of 10 pulses at 100 GeV/c.

Fig. 9 The pulse height distributions of the mean of the
 smallest 6 out of 10 pulses at 200 GeV/c.

(a)



(b)

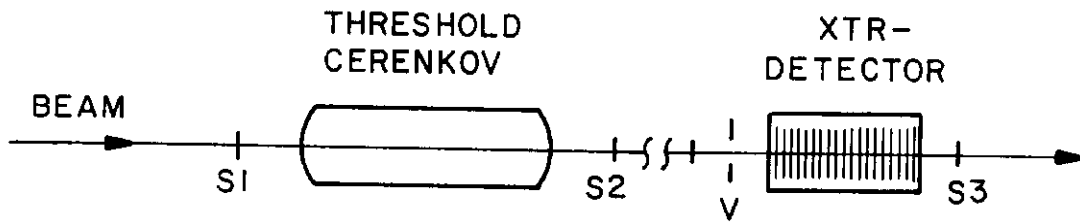


Fig. 1

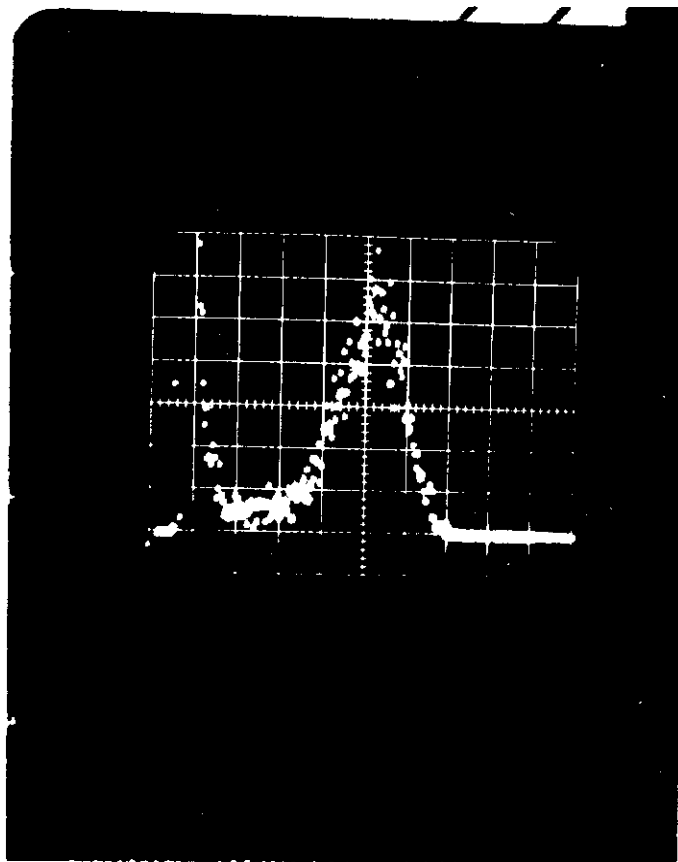


Fig. 2

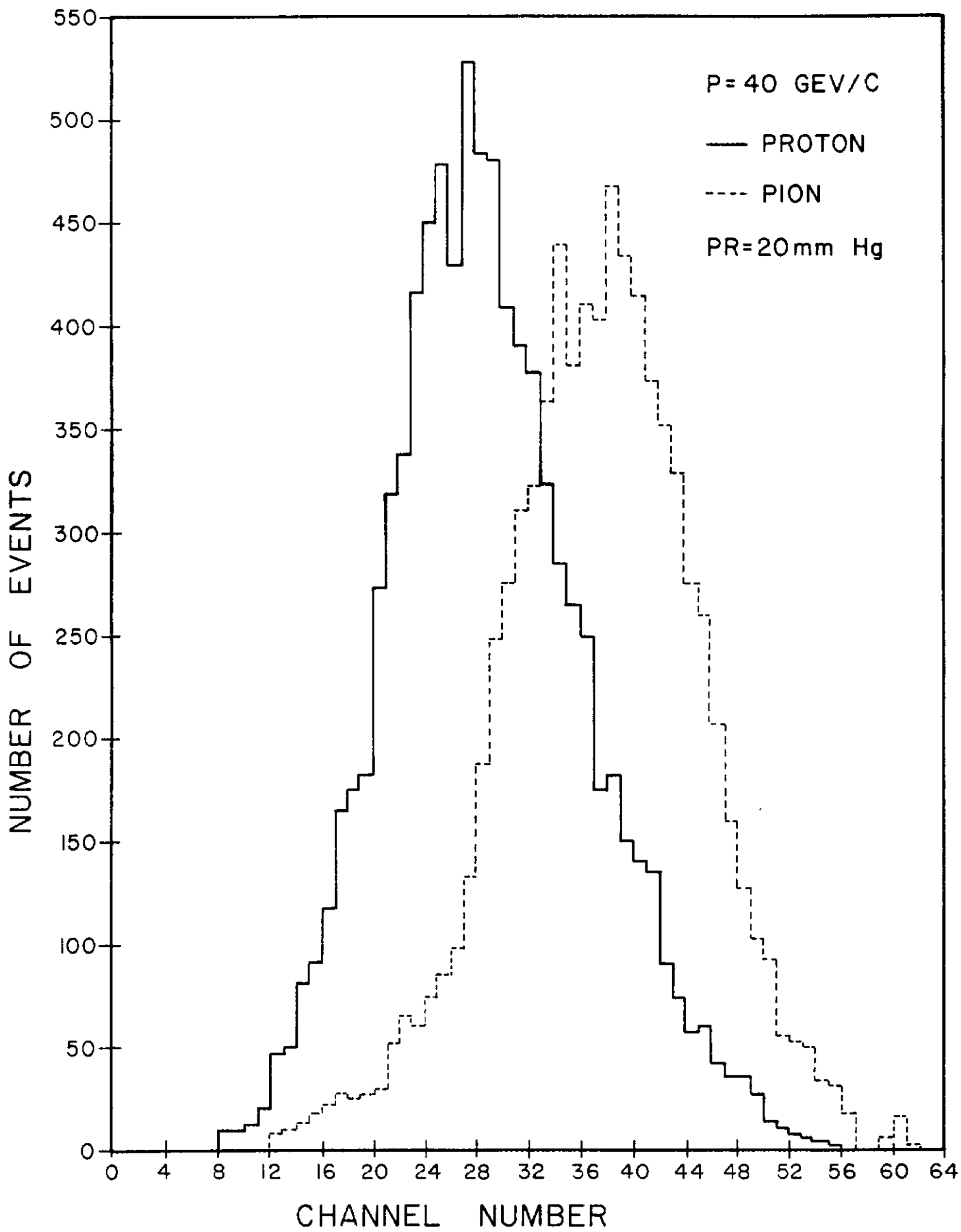


Fig. 3

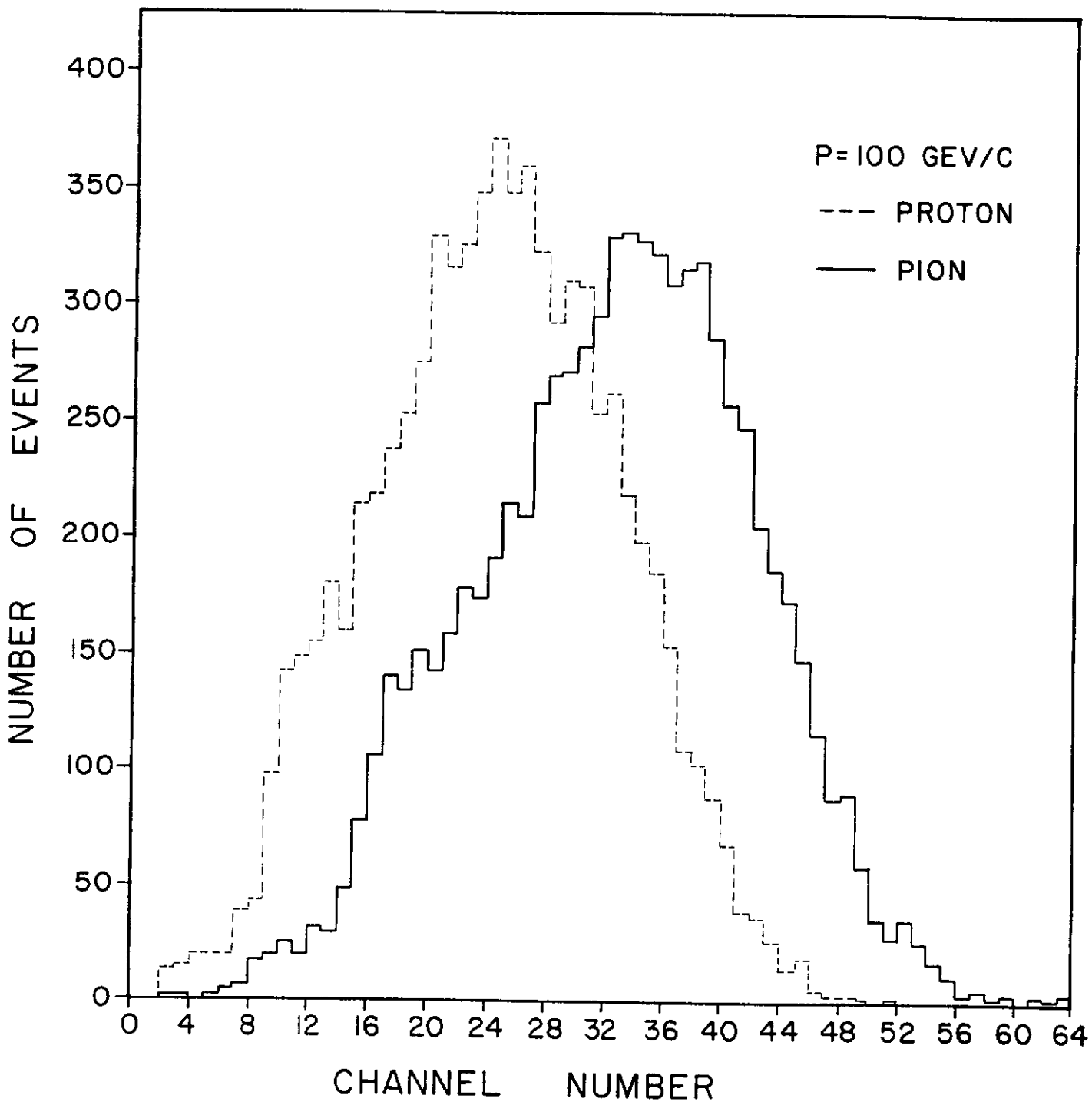


Fig. 4

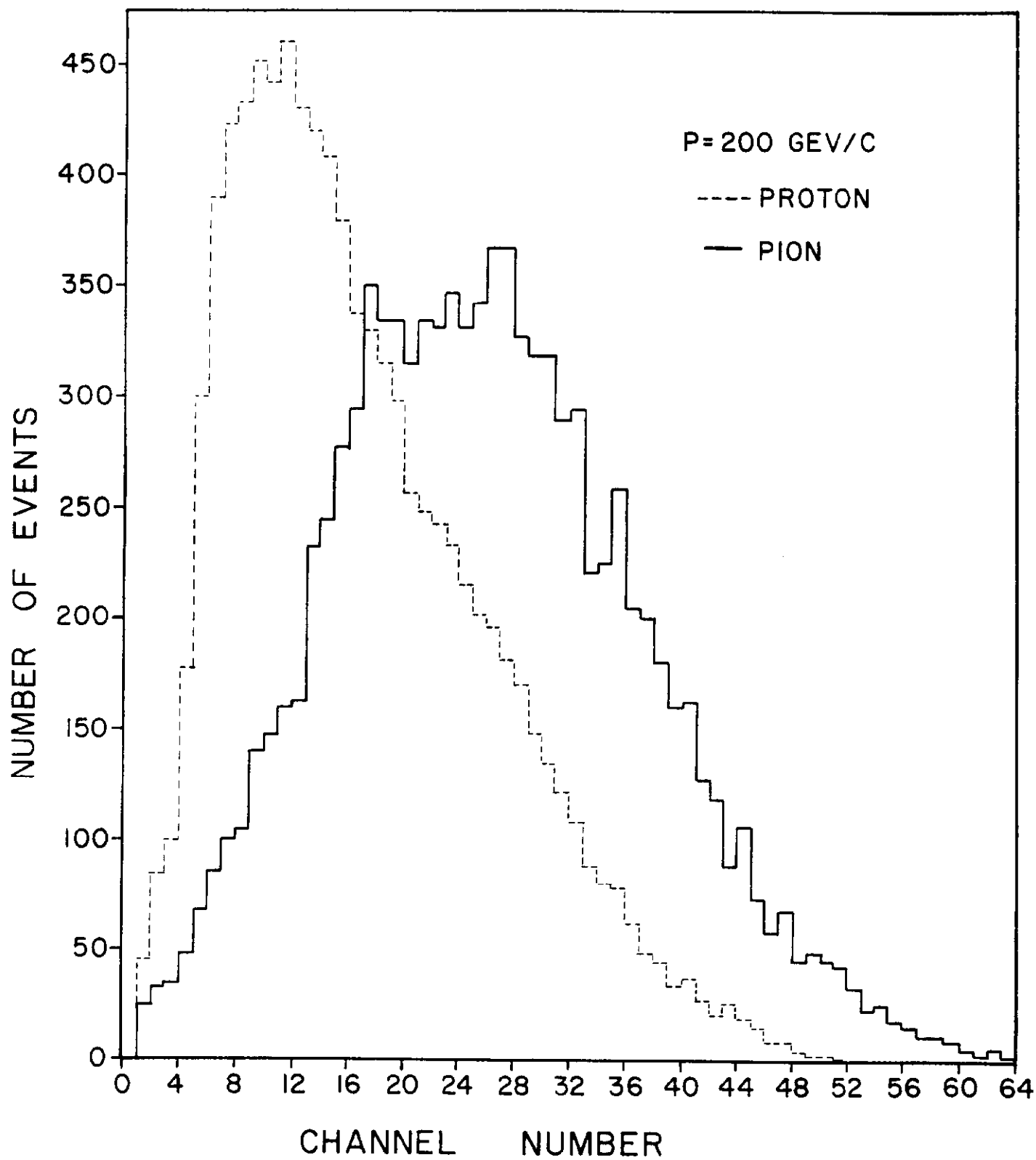


Fig. 5

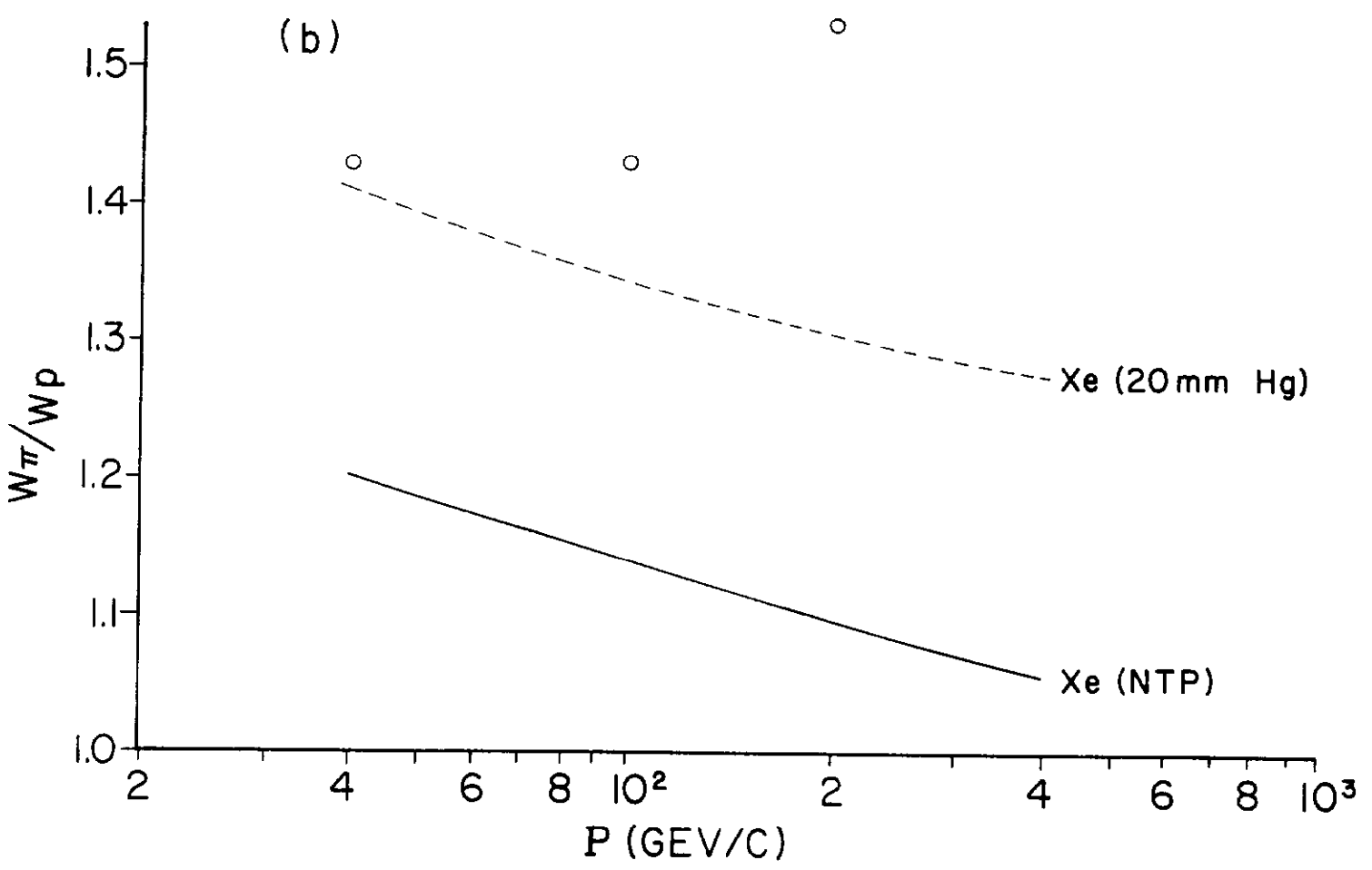
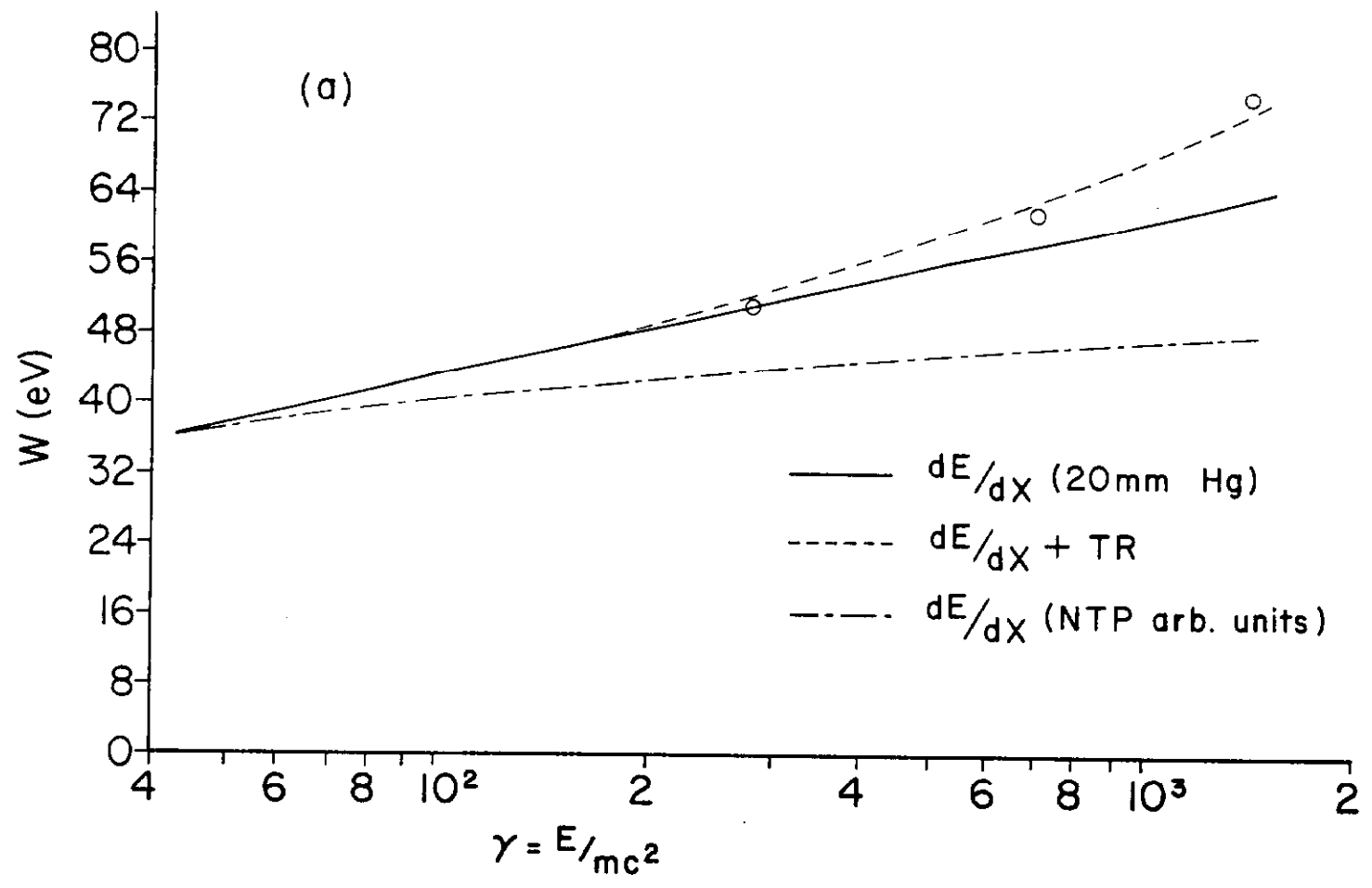


Fig. 6

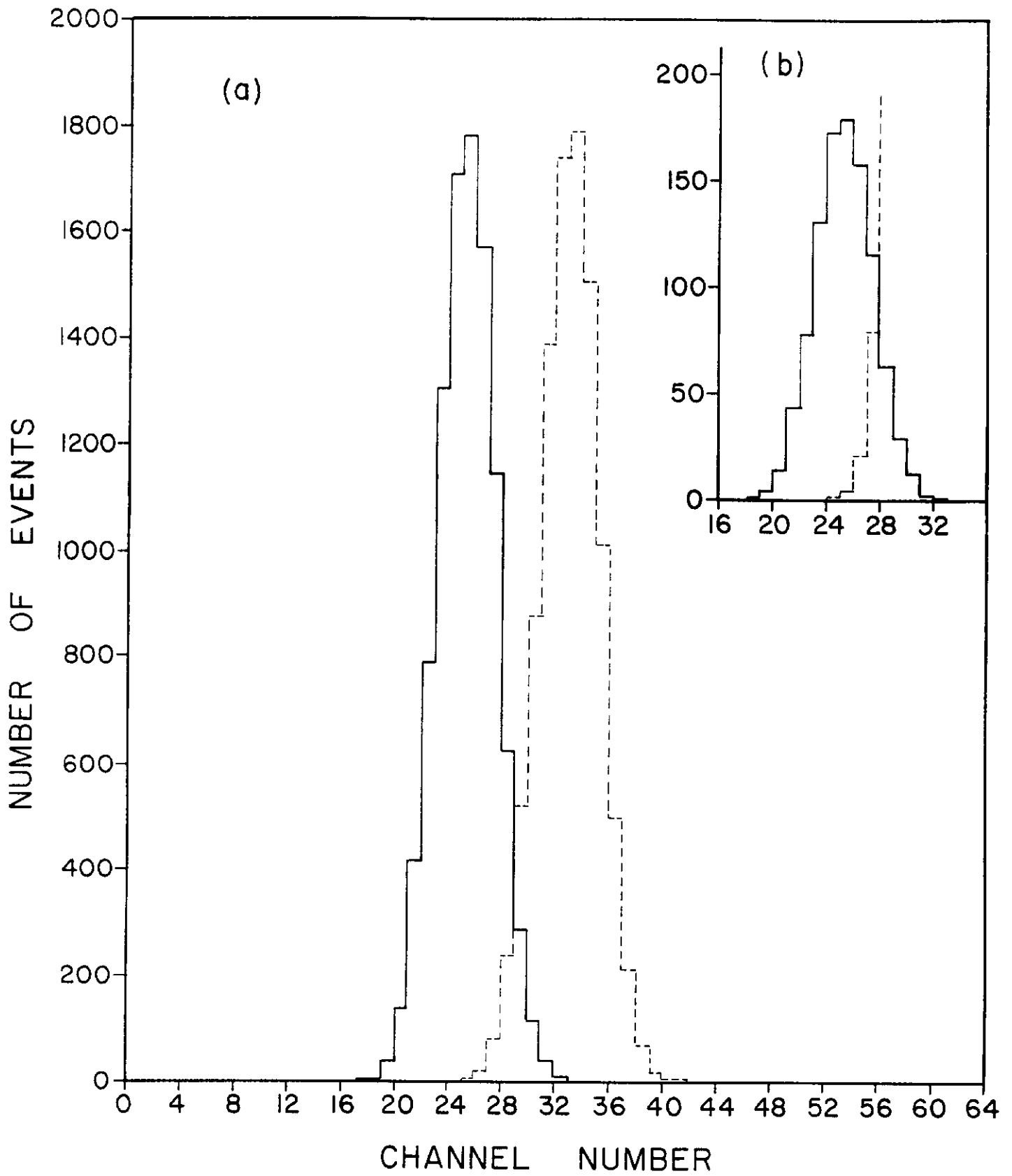


Fig. 7

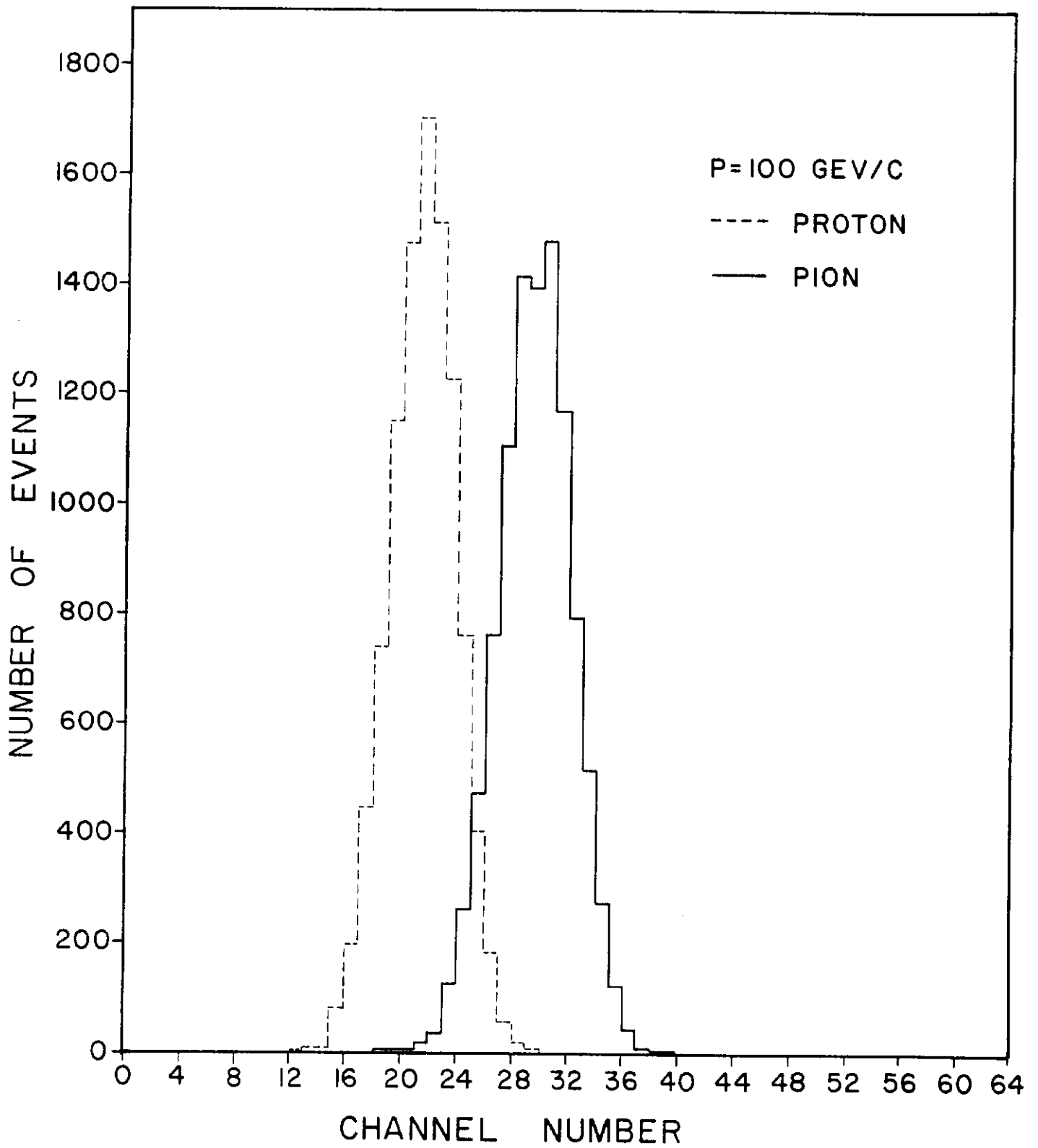


Fig. 8

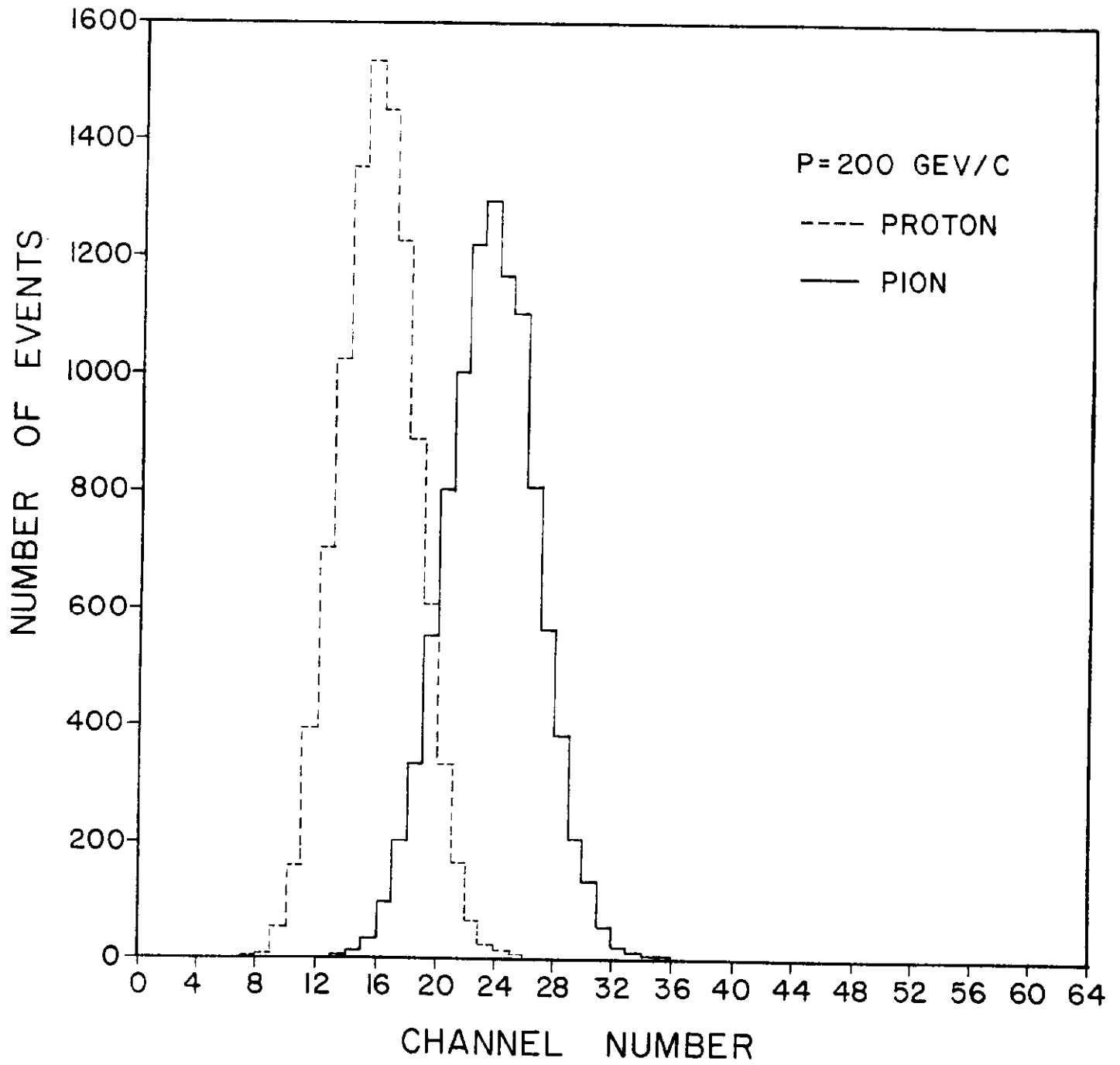


Fig. 9